2-8-2008

Climatology of mesopause region temperature, zonal wind, and meridional wind over Fort Collins,Colorado (41°N, 105°W), and comparison with model simulations

Titus Yuan
Utah State University

C. Y. She

D. A. Krueger

F. Sassi

R. Garcia

R. G. Roble

See next page for additional authors

Recommended Citation

Yuan, T., C. She, D. A. Krueger, F. Sassi, R. Garcia, R. G. Roble, H. Liu, H. Schmidt and Steven Reising (2008), Climatology of mesopause region temperature, zonal wind, and meridional wind over Fort Collins, Colorado (41°N, 105°W), and comparison with model simulations, J. Geophys. Res., 113, D03105, doi:10.1029/2007JD008697.

Climatology of mesopause region temperature, zonal wind, and meridional wind over Fort Collins, Colorado (41°N, 105°W), and comparison with model simulations

Tao Yuan,[1] Chiao-Yao She,[1] David A. Krueger,[1] Fabrizio Sassi,[2] Rolando Garcia,[2] Raymond G. Roble,[2] Han-Li Liu,[2] and Hauke Schmidt[3]

Received 22 March 2007; revised 29 August 2007; accepted 8 November 2007; published 8 February 2008.

[1] Between May 2002 and April 2006, many continuous observations of mesopause region temperature and horizontal wind, each lasting longer than 24 h (termed full-diurnal-cycle observations), were completed at the Colorado State University Na Lidar Facility in Fort Collins, Colorado (41°N, 105°W). The combined data set consists of 120 full-diurnal-cycle observations binned on a monthly basis, with a minimum of 7 cycles in April and a maximum of 18 cycles in August. Each monthly data set was analyzed to deduce mean values and tidal period perturbations. After removal of tidal signals, monthly mean values are used for the study of seasonal variations in mesopause region temperature, zonal and meridional winds. The results are in qualitative agreement with our current understanding of mean temperature and wind structures in the midlatitude mesopause region with an observed summer mesopause of 167 K at 84 km, summer peak eastward zonal wind of 48 m/s at 94 km, winter zonal wind reversal at ~95 km, and peak summer (pole) to winter (pole) meridional flow of 17 m/s at 86 km. The observed mean state in temperature, zonal and meridional winds are compared with the predictions of three current general circulation models, i.e., the Whole Atmosphere Community Climate Model version 3 (WACCM3) with two different simulations of gravity wavefields, the Hamburg Model of the Neutral and Ionized Atmosphere (HAMMONIA), and the 2003 simulation of the Thermosphere-Ionosphere-Mesosphere-Electrodynamics General Circulation Model (TIME-GCM). While general agreement is found between observation and model predictions, there exist discrepancies between model prediction and observation, as well as among predictions from different models. Specifically, the predicted summer mesopause altitude is lower by 3 km, 8 km, 3 km, and 1 km for WACCM3 the two WACCM runs, HAMMONIA, and TIME-GCM, respectively, and the corresponding temperatures are 169 K, 170 K, 158 K, and 161 K. The model predicted summer eastward zonal wind peaks to 71 m/s at 102 km, to 48 m/s at 84 km, to 75 m/s at 93 km, and to 29 m/s at 94 km, in the same order. The altitude of the winter zonal wind reversal and seasonal asymmetry of the pole-to-pole meridional flow are also compared, and the importance of full-diurnal-cycle observations for the determination of mean states is discussed.

Citation: Yuan, T., C.-Y. She, D. A. Krueger, F. Sassi, R. Garcia, R. G. Roble, H.-L. Liu, and H. Schmidt (2008), Climatology of mesopause region temperature, zonal wind, and meridional wind over Fort Collins, Colorado (41°N, 105°W), and comparison with model simulations, *J. Geophys. Res.*, *113*, D03105, doi:10.1029/2007JD008697.

1. Introduction

[2] Studies of the MLT (Mesosphere and Lower Thermosphere) have long suffered from the region's inaccessibility both to the highest-flying research balloons and to the lowest orbiting satellites. There is a growing realization that the MLT provides an important link in the vertical transfer of energy and mass in the atmosphere [*Jarvis*, 2001]. These vertical links between geospace (which extends from the ionosphere out to the Sun) and the lower atmosphere are beginning to be explored and the MLT plays an important role in the upward propagation of wave energy to the thermosphere [*Lawrence and Jarvis*, 2001]. Within the MLT, the mesopause region (from ~80 to 110 km) is defined as the transition between the mesosphere and the thermosphere and is also the coldest place

[1]Physics Department, Colorado State University, Fort Collins, Colorado, USA.
[2]National Center for Atmospheric Research, Boulder, Colorado, USA.
[3]Max Planck Institute for Meteorology, Hamburg, Germany.

0148-0227/08/2007JD008697

anywhere in Earth's atmosphere. In the mesopause region, atomic elements such as sodium (Na), potassium (K) and calcium (Ca) are generated by the ablation of meteors during their entry into the atmosphere. These elements provide neutral tracers that scientists can use to observe the chemistry and dynamics of the MLT. The Colorado State University (CSU) Na fluorescence lidar, one of the most advanced lidar systems of its kind, takes advantage of the existence of sodium atoms in the mesopause region, and has observed this part of the MLT for more than 15 years in an unprecedented manner, providing valuable data for the study of this poorly understood layer of the atmosphere.

[3] On the basis of nocturnal averages of varied duration in a night, lidar data have been used to compile climatology and deduce thermal structure of middle atmosphere and mesopause region, revealing the counterintuitive, two-level temperature structure of the mesopause worldwide [*Lübken and von Zahn*, 1991; *Yu and She*, 1995; *von Zahn and Höffner*, 1996; *She and von Zahn*, 1998]. The compilation of temperature climatology based on extensive nocturnal observations over Fort Collins, Colorado [*She et al.*, 2000], and sites at varied latitudes [*Leblanc et al.*, 1998] have been published. The study of She and coworkers reveals an annual variation with low- (high-) altitude mesopause in summer (winter), typical of high latitudes. The study of Leblanc and coworkers reveals a semiannual oscillation typical of tropical latitudes. The climatological means deduced from nocturnal observation are thought to be contaminated by diurnal tide [*States and Gardner*, 1998] and the challenge of extracting tides from observation covering a fraction of a day was already appreciated more than two decades ago [*Crary and Forbes*, 1983]. The published diurnal temperature means deduced from observations in both day and night [*States and Gardner*, 2000; *Chen et al.*, 2000], on the other hand, suffered from insufficient data as well as data gaps. At the same time, horizontal winds in the mesopause region can be measured by MF and meteor radar [*Franke and Thorsen*, 1993; *Jacobi et al.*, 2005]. Though considerable radar studies of horizontal wind tides exist in the literature [*Manson et al.*, 1989; *Pancheva et al.*, 2002], radar and satellite studies of the mean wind climatology have been rare [*Franke and Thorsen*, 1993; *Swinbank and Ortland*, 2003].

[4] The climatology we report in this paper is based not only on simultaneous observation of temperature, zonal and meridional winds, but also on full-diurnal-cycle observations, including only data sets that are continuous for more than 24 h. This data set with over 3600 h of observation is well distributed throughout the year, permitting the determination of true (or tidal removed) monthly mean temperature, zonal and meridional winds suitable for comparison with seasonal variations of the mean states derived from the General Circulation Models [see *Garcia et al.*, 2005, and references therein]. The paper is organized as follows. Lidar data distribution and analysis are given in section 2, and the importance of full-diurnal-cycle observation for climatology is illustrated with April observation in section 3. The selection and description of the 3 models, as well as the objectives of this comparison study are given in section 4, with associated the results in section 5, before the conclusions in section 6.

2. Lidar Data Distribution and Analysis

[5] The two-beam Na lidar at Colorado State University (41°N, 105°W) has observed full diurnal cycles of the mesopause region temperature and horizontal wind in campaign mode since May 2002, weather permitting [*She et al.*, 2004]. The technical innovations that incorporated a dual-path acousto-optic modulator and a Na vapor Faraday filter in the Na lidar system that allows Doppler wind measurement and observation under sunlit condition, respectively, have been described elsewhere [*Arnold and She*, 2003]. By April 2006, over 3600 h of diurnal-cycle observations had been completed. The Na lidar signals of the north and east beams, each pointing 30° from zenith, consist of photon count profiles of Na fluorescence, from which temperature, zonal and meridional winds can be deduced. The photon count profiles of each beam are first summed for each hour and vertically smoothed using a Hanning window of 2 km full-width half-maximum (FWHM) for data acquired at night, and of 4 km FWHM under sunlit conditions. The measurement uncertainty for hourly temperature and line-of-sight wind under nighttime clear-sky conditions between 84 and 100 km were estimated to be <2 K and <1.5 m/s in summer and <1 K and 1 m/s in winter, respectively. Outside this altitude range, the measurement uncertainty increases rapidly as the Na density decreasing dramatically with the uncertainty typically increasing by about a factor of 2 at 103 km from its value at 100 km, and at 81 km in winter and at 82 km in summer from its value at 84 km. The measurement error under sunlit conditions is only 1.5 times larger at dawn and sunset and up to 10 times larger at local noon, and varies between these values at other times. Assuming that the hourly mean vertical wind is negligible, hourly mean profiles of the zonal wind are determined from the east beam measurements, of the meridional wind from the north beam, and of temperature obtained from the average of the temperatures measured by the two beams.

[6] On the basis of hourly mean temperature and wind profiles from the data sets with continuous observations of 24 h or longer that were observed within a given month, the least squares fitting method is used to deduce the amplitude and phase of the diurnal, semidiurnal, terdiurnal and quadiurnal tidal components. The tide is then removed to calculate monthly mean values. The uncertainty for the monthly mean, and tidal amplitudes and phases is the result of error propagation, resulting from the measurement error (photon noise) in each hourly mean profile and geophysical variability (sometimes termed geophysical noise) that inevitably exist between hourly mean profiles in the month through the linear least squares fitting analysis. The method and the nature of the deduced uncertainty were previously discussed [*She et al.*, 2003]. The resulting uncertainty in the monthly fitting mean, depending on the abundance of the Na layer and the amount of data in each month, is expected, for this data set, to be comparable to the measurement error of a nocturnal hourly mean. Since only data from full-diurnal-cycle observation are used, the monthly means

Table 1a. Monthly Diurnal Mean Temperatures Over Fort Collins, Colorado (41°N, 105°W)

Altitude, km	TC1, K	TC2, K	TC3, K	TC4, K	TC5, K	TC6, K	TC7, K	TC8, K	TC9, K	TC10, K	TC11, K	TC12, K
76	no value	no value	no value	no value	no value	no value	no value	no value	no value	no value	no value	238.4
77	231.1	no value	no value	no value	no value	no value	no value	no value	no value	no value	226.8	232.5
78	229.4	no value	no value	no value	no value	no value	no value	no value	no value	no value	220.5	231.3
79	226.7	no value	no value	no value	no value	no value	no value	no value	no value	211.1	215.6	228.6
80	223.8	no value	196.7	no value	189.0	no value	184.6	189.7	196.5	206.1	221.9	223.4
81	220.7	199.8	196.2	no value	190.4	174.2	183.3	190.9	196.0	203.4	209.5	219.2
82	217.5	197.6	198.1	no value	187.1	171.1	178.0	187.8	194.2	201.5	207.9	217.7
83	215.0	196.3	197.3	187.7	182.7	169.4	176.9	185.7	192.7	200.9	207.3	217.0
84	212.8	194.2	196.0	187.4	179.4	167.4	176.6	184.3	191.7	201.2	206.5	216.3
85	210.6	192.6	194.7	187.1	178.4	168.2	176.6	184.2	190.9	201.6	205.5	215.2
86	208.2	192.3	193.9	186.6	177.3	169.6	177.3	184.4	190.0	201.7	204.6	213.6
87	205.3	192.4	193.4	186.1	176.6	171.9	178.4	184.6	189.3	201.9	203.9	211.5
88	202.6	192.0	192.7	185.5	176.5	173.9	179.2	184.7	188.4	201.6	203.2	209.8
89	199.7	191.4	191.7	185.0	176.7	176.1	179.7	184.8	187.2	201.0	202.0	207.9
90	196.8	190.3	190.9	184.4	177.4	178.1	180.2	184.6	186.1	200.1	200.5	205.8
91	194.4	189.1	190.2	183.6	178.2	179.6	180.6	184.4	185.0	199.2	199.1	203.8
92	191.7	187.4	189.4	182.8	179.0	180.8	180.8	183.9	184.0	198.1	197.6	201.3
93	189.1	185.4	188.5	181.9	179.2	181.4	180.7	183.0	183.1	196.8	195.7	198.7
94	186.6	183.4	187.5	181.0	179.1	181.2	180.4	182.1	182.3	195.6	193.6	196.0
95	184.5	181.8	186.5	180.2	178.3	181.0	180.1	181.3	181.6	194.3	191.8	193.4
96	182.2	180.2	185.1	178.3	179.0	179.8	179.7	180.2	180.8	192.7	190.0	190.3
97	179.7	178.5	184.0	177.5	178.4	180.4	179.3	179.3	180.1	191.0	188.6	187.3
98	177.7	177.8	183.0	176.2	178.9	168.1	178.5	178.1	179.0	189.2	187.2	184.9
99	175.9	176.8	182.6	177.1	178.5	no value	178.4	176.5	177.4	187.6	185.8	182.4
100	174.3	177.1	181.8	177.9	179.9	no value	179.2	174.7	175.8	186.0	184.6	180.2
101	173.2	178.9	181.0	179.0	no value	no value	no value	no value	175.1	184.3	183.7	178.4
102	174.3	no value	177.9	no value	no value	no value	no value	no value	no value	183.1	184.1	177.4
103	176.9	no value	no value	no value	no value	no value	no value	no value	no value	182.1	185.3	176.4
104	no value	no value	no value	no value	no value	no value	no value	no value	no value	179.0	no value	179.1
Average uncertainty	0.82	0.82	0.85	0.86	0.99	0.81	0.92	0.75	0.63	0.80	0.80	0.91

deduced from the linear least squares fitting program are identical to those deduced from straight average of the monthly data, except at the edges of the Na layer, where the error bars of nighttime measurements are much smaller than those under sunlit condition. In this paper, we tabulate the mean state values in Tables 1a–1c, and limit the reporting altitudes to include only those monthly fitting means with small uncertainty, i.e., less than 3 K, 10 m/s and 5 m/s for temperature, zonal and meridional winds, respectively. The average uncertainty of the observation altitude range is also reported for each month in Tables 1a–1c.

[7] The data distribution for each month during this period is shown in Figure 1. Different colors represent the number of hours of data for the years 2002 to 2006. The shortest data set was in April, still longer than 7 d. The maximum amount of data was in August, nearly 18 d.

3. Significance of Full-Diurnal-Cycle Observation

[8] Because of the prevalence of tidal period perturbations (24, 12, and 8 h) in the mesopause region, the importance and necessity of observation over complete diurnal cycles for the purpose of establishing mean state climatology cannot be underestimated. The strong bias and influence of tidal perturbations on the mean state based on averages from nighttime observation of varied duration can best be illustrated by comparing averages over different periods in a day and by examining the tidal amplitudes and phases derived from data of full-diurnal-cycle observation. Here, we use the month of April as an example, because the Na abundance in April is representative of the annual mean, being higher than the summer values and lower than those in winter.

[9] Figure 2 shows the vertical profiles of monthly mean temperature, zonal and meridional winds for April in Figures 2a, 2b, and 2c, respectively, along with the associated 12-h averages between 1800 and 0600 LST (local solar time), and between 0600 and 1800 LST, designated as nighttime average and daytime average, respectively. In Figure 2a, the 8-year nocturnal April mean temperature based on observations between 1991 and 1999 [*She et al.*, 2000] is also included for comparison. Since April consists of only 7 cycles of full-diurnal observations, we restrict our reporting altitudes to be consistent with those in Tables 1a–1c with uncertainties of less than 3 K, 10 m/s and 5 m/s for diurnal mean temperature, zonal and meridional winds, respectively.

[10] We note in Figure 2a that the diurnal mean temperature between 88 and 100 km is higher (lower) than the daytime (nighttime) average by as much as 8 K; the opposite is true for altitudes between 84 and 88 km but with a smaller difference of less than 4 K. Clearly, the main difference between the diurnal, nighttime and daytime means is due to the diurnal tide [*Yuan et al.*, 2006]. The fact that the diurnal temperature tide peaks in the nighttime (daytime) hours above (below) 88 km with an amplitude of ~5 K between 84 and 95 km, which increases to ~8 K at 100 km, as shown in Figures 2d and 2e, can approximately explain the differences among the 3 means. However, the temperature of the 8-year nocturnal mean at 90 km is higher than the diurnal mean by ~9 K. To account for this difference, we note that the data from nocturnal observation

Table 1b. Monthly Diurnal Mean Zonal Winds Over Fort Collins, Colorado (41°N, 105°W)

Altitude, km	U1, m s^{-1}	U2, m s^{-1}	U3, m s^{-1}	U4, m s^{-1}	U5, m s^{-1}	U6, m s^{-1}	U7, m s^{-1}	U8, m s^{-1}	U9, m s^{-1}	U10, m s^{-1}	U11, m s^{-1}	U12, m s^{-1}
76	48.9	no value	no value	no value	no value	no value	no value	no value	no value	no value	no value	37.4
77	43.7	no value	no value	no value	no value	no value	no value	no value	no value	no value	37.4	41.1
78	43.3	no value	no value	no value	no value	no value	no value	no value	no value	20.0	33.6	38.9
79	42.0	no value	no value	no value	no value	no value	no value	no value	no value	21.7	30.3	39.0
80	40.8	no value	18.9	no value	no value	no value	no value	no value	5.8	16.7	25.5	36.3
81	40.7	29.2	14.6	no value	−22.3	no value	no value	−2.5	14.8	13.6	22.5	33.1
82	38.8	24.1	10.4	14.2	−20.2	−19.3	3.0	5.6	13.7	13.5	20.8	31.5
83	36.0	23.8	7.0	3.1	−13.3	3.7	8.4	8.2	13.4	10.1	19.1	30.5
84	33.0	21.9	6.2	−8.4	−8.4	12.1	10.8	9.3	12.8	8.0	17.1	29.7
85	29.7	22.5	5.3	−8.8	−3.2	15.7	15.1	11.9	10.6	5.8	14.9	27.6
86	26.1	23.9	4.4	−10.8	4.3	21.2	19.5	13.9	9.7	3.4	13.4	24.1
87	21.5	25.8	2.7	−11.1	9.9	26.3	22.9	14.5	9.3	1.9	12.1	20.3
88	17.5	27.7	0.8	−9.6	15.0	30.2	25.9	15.0	8.6	1.4	10.5	16.6
89	13.5	29.2	−1.0	−9.1	20.7	35.5	29.0	15.7	7.4	1.0	8.0	12.3
90	10.7	29.0	−2.1	−8.2	25.6	39.1	31.5	16.7	5.7	0.9	5.6	8.7
91	9.1	28.6	−2.5	−7.6	29.1	41.9	32.7	17.6	3.6	0.4	3.8	6.3
92	7.1	27.4	−2.4	−6.8	32.5	43.7	33.5	18.5	1.3	−0.2	2.1	4.5
93	5.3	24.4	−2.4	−5.7	34.1	45.6	34.1	19.1	−0.6	−0.4	1.0	3.2
94	3.8	21.3	−2.5	−4.4	36.9	47.6	34.2	19.4	−1.7	−0.2	0.5	1.8
95	2.2	16.9	−3.0	−2.9	36.9	46.7	33.3	19.1	−2.4	−0.0	0.4	0.3
96	−0.5	16.0	−4.5	−1.8	35.8	46.7	30.4	17.8	−3.5	−1.2	0.1	−1.7
97	−3.8	15.5	−6.5	0.2	36.9	no value	26.6	15.7	−5.4	−2.2	−1.7	−4.1
98	−6.2	12.8	−9.4	2.6	41.7	no value	22.2	11.9	−5.2	−3.0	−3.7	−6.8
99	−8.0	9.5	−13.4	6.4	44.2	no value	16.7	9.7	−7.7	−3.6	−6.8	−10.1
100	−7.6	5.1	−16.4	no value	52.4	no value	13.3	6.8	−11.9	−1.9	−11.9	−15.0
101	−8.3	−2.4	−18.9	no value	no value	no value	no value	no value	no value	−2.9	−15.6	−19.6
102	−9.1	no value	no value	no value	no value	no value	no value	no value	no value	−2.4	−22.2	−23.0
103	no value	no value	no value	no value	no value	no value	no value	no value	no value	−7.0	−30.5	−21.1
104	no value	no value	no value	no value	no value	no value	no value	no value	no value	no value	no value	−28.8
Average uncertainty	2.9	2.7	2.3	3.0	2.7	2.8	2.4	1.9	2.0	2.4	2.1	2.8

Table 1c. Monthly Diurnal Meridional Winds Over Fort Collins, Colorado (41°N, 105°W)

Altitude, km	V1, m s^{-1}	V2, m s^{-1}	V3, m s^{-1}	V4, m s^{-1}	V5, m s^{-1}	V6, m s^{-1}	V7, m s^{-1}	V8, m s^{-1}	V9, m s^{-1}	V10, m s^{-1}	V11, m s^{-1}	V12, m s^{-1}
76	no value	no value	no value	no value	no value	no value	no value	no value	no value	no value	no value	no value
77	8.7	no value	no value	no value	no value	no value	no value	no value	no value	no value	4.4	4.2
78	11.6	no value	no value	no value	no value	no value	no value	no value	no value	no value	4.7	6.3
79	13.4	no value	no value	no value	no value	no value	no value	no value	no value	2.0	4.6	2.7
80	14.3	no value	no value	no value	no value	no value	no value	10.8	no value	2.0	4.9	3.0
81	14.9	no value	no value	no value	−9.2	no value	−2.0	6.6	2.4	2.2	3.6	3.2
82	13.3	5.5	6.7	no value	−11.4	−12.3	−2.5	3.5	2.9	2.6	2.5	6.3
83	12.6	4.9	1.4	−10.0	−12.8	−14.8	−4.5	−0.2	2.6	1.2	0.9	6.1
84	11.6	4.4	0.1	−5.7	−14.7	−14.9	−6.0	−0.3	3.5	−0.9	0.2	6.3
85	10.2	4.1	−2.2	−2.7	−16.6	−13.7	−6.6	−1.8	3.5	−2.3	0.2	5.9
86	8.5	4.5	−3.0	−1.6	−16.8	−12.2	−4.7	−3.0	2.4	−3.3	0.8	5.2
87	6.8	4.3	−4.0	−1.7	−16.7	−11.7	−5.1	−3.7	0.7	−2.9	1.1	4.8
88	5.6	3.5	−4.9	−1.0	−16.3	−10.5	−5.9	−3.8	−0.6	−2.3	0.9	5.1
89	4.2	2.5	−4.5	−0.1	−15.3	−7.6	−6.4	−3.2	−1.4	−1.7	0.3	5.6
90	2.4	2.0	−2.8	0.7	−15.4	−4.6	−6.5	−2.7	−1.9	−0.9	−0.1	5.7
91	0.4	1.5	−0.7	1.4	−15.6	−2.8	−6.1	−2.1	−2.5	0.0	−0.5	5.6
92	−2.2	0.6	1.4	2.2	−15.6	−1.3	−5.3	−1.9	−3.4	0.7	−0.4	6.1
93	−4.1	0.1	2.8	2.9	−15.2	0.0	−4.8	−2.2	−3.8	0.7	0.6	6.4
94	−5.1	0.8	3.5	3.5	−15.3	0.7	−4.8	−2.9	−3.6	0.0	1.6	6.3
95	−5.3	1.5	3.4	3.2	−16.3	1.3	−5.1	−3.5	−3.3	−0.7	2.1	6.0
96	−4.9	3.1	2.9	2.4	−13.5	2.0	−5.2	−4.2	−2.6	−1.5	0.8	5.0
97	−3.8	5.2	2.0	1.7	−11.9	2.5	−3.4	−5.0	−2.0	−2.8	−0.2	3.6
98	−2.4	7.8	0.7	1.2	−10.9	no value	−2.1	−1.7	−2.2	−2.6	−1.1	2.2
99	−1.1	8.0	−2.1	1.0	−8.7	no value	−0.1	2.6	−3.0	−2.2	−1.2	0.5
100	−0.4	8.3	−5.8	−2.7	no value	no value	no value	7.0	−4.7	−2.0	−1.0	−0.3
101	1.1	12.4	−5.0	no value	no value	no value	no value	no value	no value	−1.3	0.7	−0.8
102	2.0	no value	no value	no value	no value	no value	no value	no value	no value	−2.2	1.8	−1.5
103	3.1	no value	no value	no value	no value	no value	no value	no value	no value	no value	3.1	−5.9
104	no value	no value	no value	no value	no value	no value	no value	no value	no value	no value	no value	no value
Average uncertainty	2.4	2.2	2	2.6	2.3	2.3	2.5	1.9	1.9	1.9	2	2.2

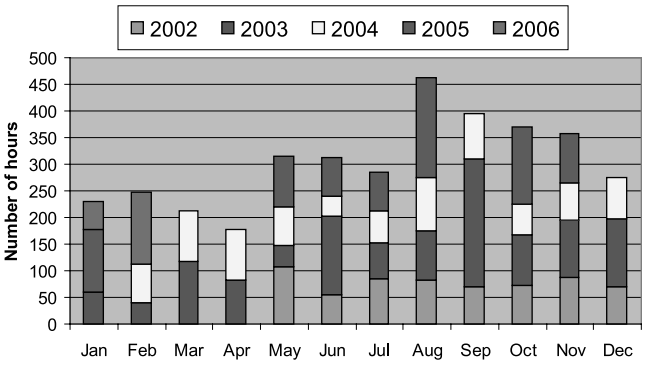

Figure 1. Quantity of Na-lidar full-diurnal observations in each moth of the year (May 2002 to April 2006).

of varied duration are most likely centered about the midnight. Since, at 90 km, the diurnal tide of 5 K peaks at ~0300 LST, and the semidiurnal tide of 3.5 K peaks at midnight (or midday), see Figures 2d and 2e, together they could arguably account for most of the difference of 9 K. We acknowledge the difficulty in comparing nocturnal mean to the diurnal mean, especially for data sets from different observational periods (1991–1999 versus 2002–2006), since both solar flux variability and global change [*Schmidt et al.*, 2006] may play a role. Nonetheless, from this example we conclude that the tidal effects are mainly responsible for the differences deduced from data sets that cover only part of a full-diurnal cycle. This tidal behavior gives rise to a warmer night observed in Figure 2a, which is also consistent with the effect of in situ nighttime chemical heating [*Mlynczak and Solomon*, 1993].

[11] The tidal effects also influence mean zonal and meridional winds. Shown in Figures 2b and 2c are the comparison between diurnal, nighttime and daytime means of the horizontal wind field; the impact of diurnal tide again is clear. Although the diurnal mean meridional wind is much smaller than that of the zonal wind, the magnitude of their tidal perturbations is comparable. The meridional wind tidal amplitudes for April are shown in Figure 2f. Here, note the typical tidal behavior in a midlatitude location with semidiurnal tide dominance above 90 km and diurnal tide dominance below 90 km, with smaller amplitudes for terdiurnal and quadiurnal tides. The altitude dependence and the amplitude of zonal wind tides (not shown) are in fact comparable. This shows the importance of full-diurnal-cycle observation for the determination of mean state climatology and points out the significant differences between the diurnal mean and nighttime averages, which were typically deduced from data between 2000 and 2400 LST. If the climatology is deduced from observations at the same local time, say at the midnight, as practiced in rocket-falling sphere measurements [*Lübken*, 1999], it then should be treated as climatology at a specified tidal phase, whose seasonal variation includes both variations of the tidal phase, and the mean state.

4. Description of Models

[12] Meteorologists have traditionally produced global circulation models that incorporate the troposphere and

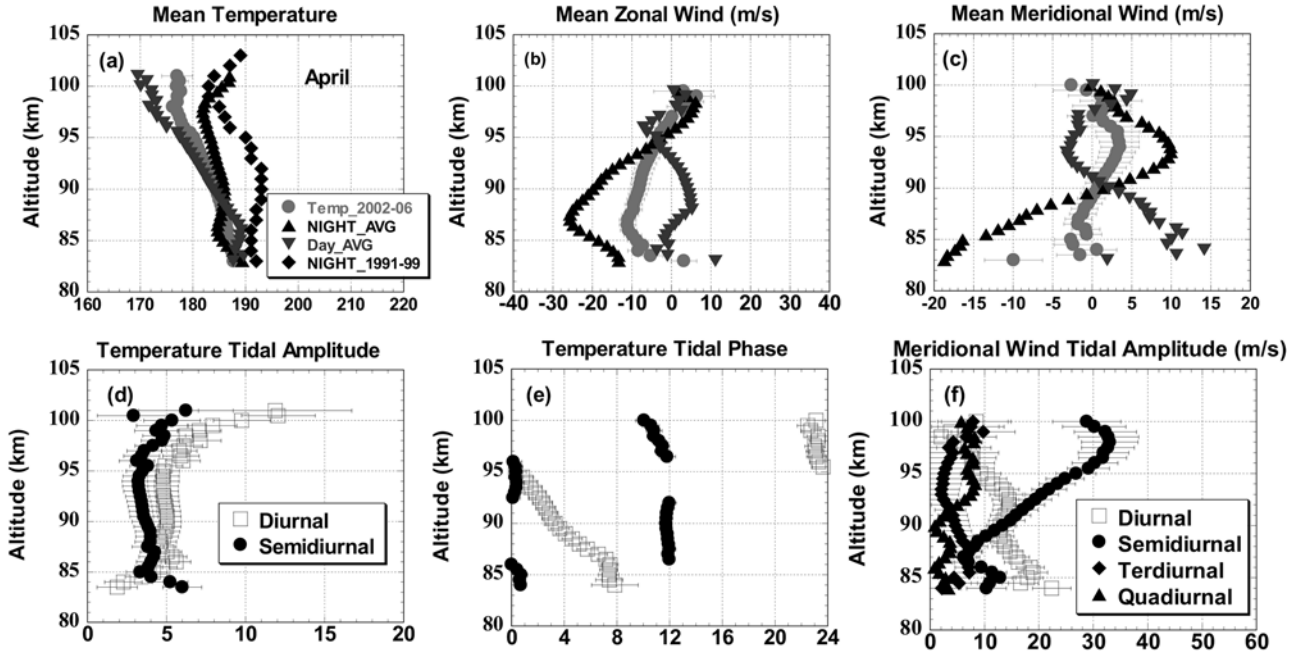

Figure 2. Climatology in the mesopause region observed by Na-lidar at Colorado State University during the month of April. (a) Comparison of diurnal mean (solid circles with uncertainty bars) and 8-year nocturnal mean (diamonds), along with daytime average (0600–1800 LST, downward triangles) and nighttime average (1800–0600 LST, upward triangles) temperatures. (b and c) Diurnal mean, daytime average and nighttime average zonal and meridional winds, respectively. (d and e) Amplitudes and phases of temperature diurnal and semidiurnal tides and (f) amplitudes of diurnal, semidiurnal, terdiurnal, and quadiurnal me al wind tides.

stratosphere (surface to ~50 km), whereas space physicists have produced global models incorporating the ionosphere, and thermosphere (from ~100 to ~500 km). The current challenge is to develop a comprehensive atmospheric model that covers the whole Earth atmosphere from the surface up to the thermosphere [*Roble*, 2000]. The MLT region dynamics is the key for the success of such model. An ambitious modeling initiative, called the Whole Atmosphere Community Climate Model (WACCM), is underway at the National Center for Atmospheric Research in Boulder, Colorado, to bridge this gap and has as its goal the simulation of the physics and chemistry of the atmosphere from the ground to the thermosphere. The Whole Atmosphere Community Climate Model version 3 (WACCM3) is a comprehensive model that extends from the Earth's surface to the lower thermosphere (~150 km). WACCM3 includes a detailed description of the troposphere using the physical parameterizations of the NCAR Community Atmosphere Model (CAM3), and the chemistry of the middle atmosphere using the Model of Ozone and Related Chemical Tracers 3 (MOZART-3) scheme (48 compounds, 153 gas phase reactions in the version used here [see *Kinnison et al.*, 2007]). WACCM3 implements a Lindzen gravity wave (GW) parameterization scheme [*Lindzen*, 1981] to represent a spectrum of waves with phase speed from −80 to +80 m/s (positive velocity is eastward, negative velocity is westward), launched from the middle troposphere at 500 hPa (~5.5 km). The source spectrum is defined ad hoc to produce realistic wind and temperature climatologies in the stratosphere and mesosphere and includes a seasonal cycle and a latitudinal structure for additional realism. In the standard implementation, the maximum source stress is exerted at the phase velocity that matches the magnitude of the wind at source level and has a Gaussian profile in phase velocity. Two simulations are presented here: a reference simulation (''ref'') in which the spectrum is used in its standard implementation [*Garcia et al.*, 2007], and a second simulation in which the maximum source stress is not shifted to match the wind at the source but is exerted at zero phase speed (''uns''). The results presented are obtained from a 20-year simulation under solar minimum conditions. While there is flexibility in the GW wave parameterization used in WACCM, the present tuning is not necessarily optimal. A sensitivity study of the middle atmosphere upon several different parameterizations of GW momentum drag has just been completed (F. Sassi et al., A sensitivity study of the middle atmosphere to changes in the parameterized momentum drag of gravity waves, submitted to *Journal of Geophysical Research,* 2007).

[13] The second GCM considered in this work is the Hamburg Model of the Neutral and Ionized Atmosphere (HAMMONIA). Its structure, complexity and purpose are similar to WACCM. HAMMONIA extends from the surface to the thermosphere, up to about 250 km. HAMMONIA is a chemistry climate model (CCM) that combines dynamics and physics from the ECHAM5/MAECHAM5 (European Centre Hamburg Model 5/Middle Atmosphere European Centre Hamburg Model 5) general circulation model [*Roeckner et al.*, 2006] along with the MOZART3 chemistry scheme and several parameterizations to account for important processes in the upper atmosphere, such as solar heating at very short w gths (UV and EUV), non-LTE (local thermal equilibrium) effects in the infrared cooling, molecular diffusion, and the ion drag. Gravity waves are parameterized and launched at 700 hPa (~3 km), using a method proposed by *Hines* [1997a, 1997b] for waves of nonorographic origin. Like WACCM3, the planetary wave effect in HAMONNIA also comes from self-consistently generated lower-atmosphere dynamics down to the Earth's surface. The results presented here are obtained from a 20-year simulation for present-day solar minimum conditions, as described by *Schmidt et al.* [2006]. Vertical resolution in the mesopause region is about 2 to 3 km.

[14] The third and final GCM for comparison is the Thermosphere-Ionosphere-Mesosphere-Electrodynamics General Circulation Model (TIME-GCM). It is a self-consistent GCM using solar forcing specified by daily solar F10.7 and it includes most of the known chemistry in the mesosphere, thermosphere and ionosphere. The CO_2 infrared cooling parameterization by *Fomichev and Shved* [1998] is used to account for a variable CO_2 mixing ratio that is important for a non-LTE process. In the thermosphere and ionosphere, auroral inputs of particle precipitation and cross-polar cap potential drop are parameterized according to the 3-h K_p index. Unlike the other two models considered in this study, TIME-GCM has a lower boundary in the middle stratosphere and extends to the upper thermosphere. In the simulations employed here, the lower boundary at 10 hPa (~30 km) is specified using daily National Center for Environmental Prediction (NCEP) reanalysis data of geopotential height and temperature. The daily sampling cannot account for PW with periods shorter than 2 d or any tidal waves. The atmospheric solar thermal tides at 10 hPa are also specified at the lower boundary, from the Global Scale Wave Model (GSWM) [*Hagan et al.*, 1999]. Similar to WACCM, a Lindzen type gravity wave (GW) parameterization scheme with a discrete spectrum of gravity waves (phase speed from −60 to 60 m s^{-1} at 10 m s^{-1} intervals) of Gaussian spectral shape are specified at the lower boundary [*Liu and Roble*, 2005]. Previous work [*Liu and Roble*, 2002] indicates that the zonal gravity wave spectrum needs to be anisotropic with the spectral peak at eastward 10 m s^{-1} (but with the meridional spectrum still isotropic), so that the simulated wind agree with the UARS wind measurements [*McLandress et al.*, 1996]. The altitude range covered by the model is 30−500 km, with the mesosphere/lower thermosphere near the center of its numerical grid, allowing dynamical, chemical, and electrodynamical coupling between the thermosphere and mesosphere to occur without major boundary influences. The TIME-GCM data presented in this paper is based on the simulation with NCEP reanalysis input of 2003, so we name it as TIME-GCM 2003 simulation.

5. Comparison of Observations With Models

[15] In this section, we compare observations with model predictions using altitude-month contour plots. Among the many unique features of mesopause dynamics, the most interesting are the lower and colder summer mesopause, the higher and warmer winter mesopause, the reversal of zonal wind direction, and reversal of the pole-to-pole meridional wind direction between winter and summer. In what follows, we will focus our discussion on the differences in

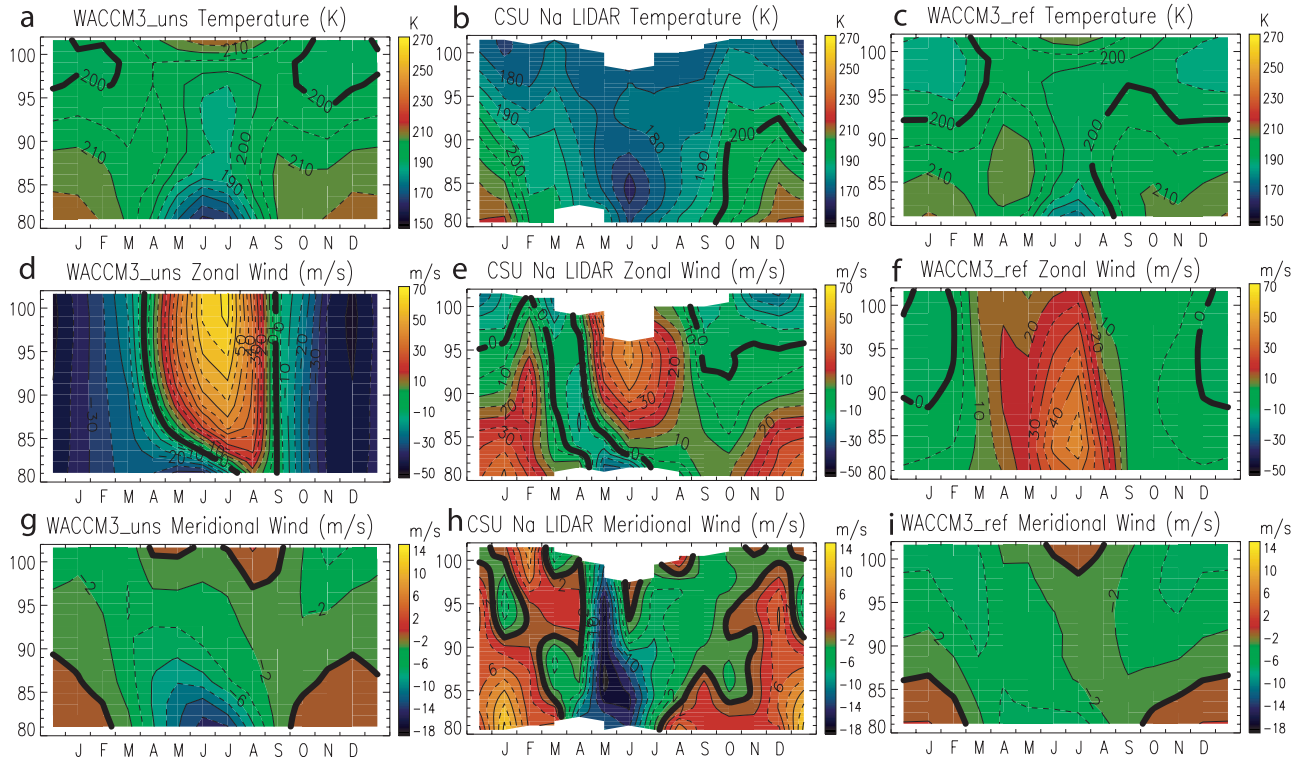

Figure 3. Comparison between Na-lidar observations with WACCM3 predictions. (a–c) Temperature, (d–f) zonal wind, and (g–i) meridional wind. Figures 3a, 3d, and 3g are for WACCM3_"uns"; Figures 3b, 3e, and 3h are for Na_lidar; and Figures 3c, 3f, and 3i are for WACCM3_"ref." Positive winds are eastward for zonal wind and northward for meridional wind.

these features between observation and model predictions. To highlight the behavior, we mark the 200 K, 0 m/s line with bold lines in these contours. In lidar observations the geometric height is determined directly from the laser pulse time of flight, whereas models tend to employ either geopotential height or (isobaric) log-pressure altitude. In this study HAMMONIA makes a conversion from geopotential height to geometric height while WACCM and TIME-GCM do not. We note that even though there are differences between the geopotential height and geometric height (at 100 km, the geometric height is about ~1.5 km higher than the geopotential height and this difference will get smaller in lower altitudes); these differences are considered minor in this paper because they are relatively much smaller than the discrepancies between model-observation and model-model comparisons as discussed below. In the contour plots, the altitudes used are geometric heights for both lidar and HAMMONIA, while they are geopotential heights for WACCM3 and TIME-GCM. However, we will use equivalent geometric heights for both WACCM3 and TIME-GCM in the discussion below. Other differences between the models include the fact that both HAMMONIA and WACCM3 provide zonally averaged monthly mean at 41°N, while TIME-GCM is the monthly mean based on 1 year (2003) simulation at a location (42.5°N, 105°W) close to Fort Collins, Colorado. The contours from lidar observations are shown in Figures 3b, 3e, 3h, 4b, 4e, and 4h, with temperature, zonal and meridional winds in Figures 3b and 4b, Figures 3e and 4e, and Figures 3h and 4h, respectively.

5.1. Comparison of Lidar Observations With WACCM3

[16] Figure 3 shows the comparison between lidar data and WACCM3 results using two versions of GW simulations. Glancing over these two versions of WACCM3 (Figures 3a, 3d, 3g, 3c, 3f, and 3i), it is evident that various GW simulation schemes in the model can generate dramatic differences. The temperature contours (Figures 3a–3c) show that the model predictions ("uns" in Figures 3a, 3d, and 3g and "ref" in Figures 3c, 3f, and 3i) and the lidar observations (Figures 3b, 3e, and 3h) exhibit similar temperature seasonal variations: cold and lower-altitude summer mesopause, and warmer and higher-altitude winter mesopause. The thermal structure of the "uns" simulation is better in this regard. The lidar summer mesopause temperature is 167 K, observed in June at 84 km. This may be comparable to the "uns" simulation of WACCM3, which yields a summer mesopause (i.e., altitude of minimum temperature) that is 3 km lower and 1 K warmer in June, compared with lidar results. For the standard gravity wave simulation ("ref" version), the summer mesopause is even lower (by 8 km relative to lidar) and about 2.5 K warmer at the same month. During the winter, the mesopause location is again higher in the lidar observations (at 101 km, 173 K in January) than in WACCM3 results (99 km, in January). The winter mesopause temperature observed by lidar is about 19 (24) K colder than the prediction from "ref" ("uns"). As was the case for temperature, both the model and the lidar data show clear summer-winter difference in the zonal wind field (Figures 3d–3f), i.e.,

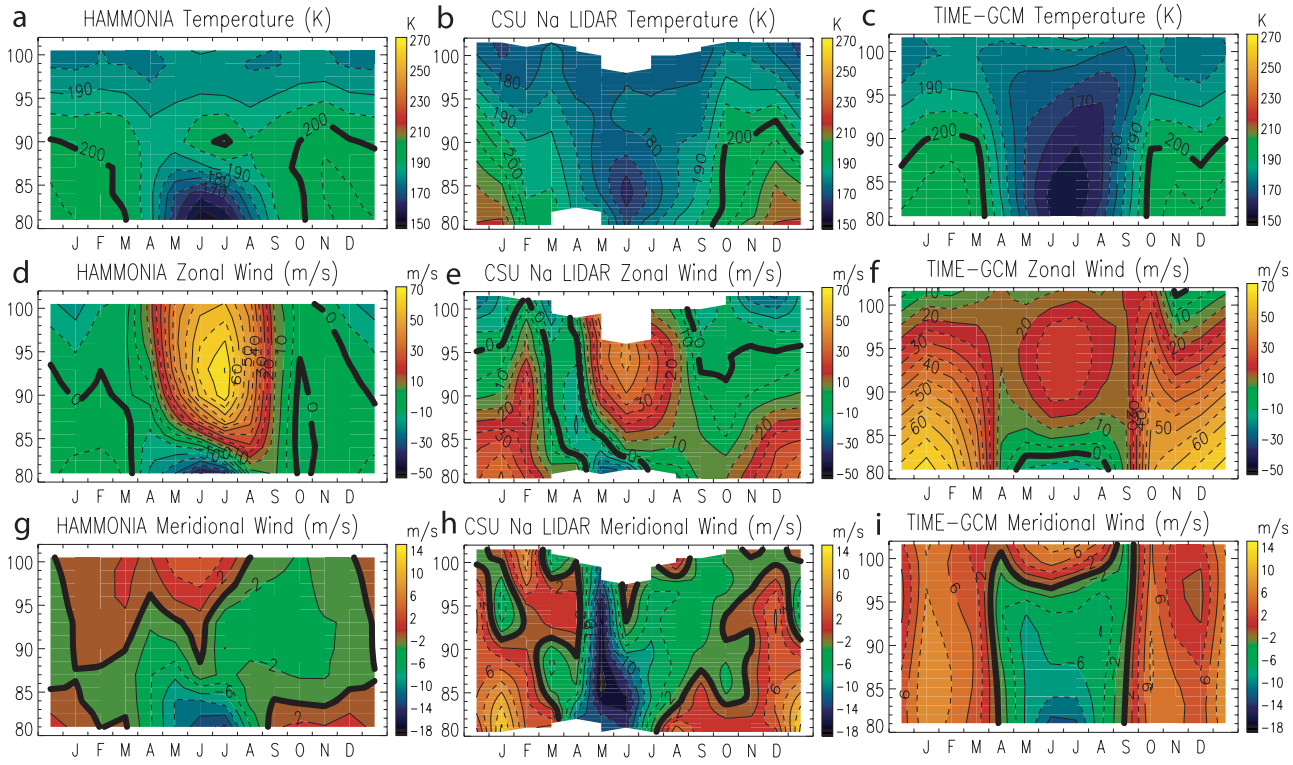

Figure 4. Comparison between Na-lidar with HAMMONIA and TIME-GCM predictions. (a–c) Temperature, (d–f) zonal wind, and (g–i) meridional wind. Figures 4a, 4d, and 4g are for HAMMONIA; Figures 4b, 4e, and 4h are for Na_lidar; and Figures 4c, 4f, and 4i are for TIME-GCM. Positive winds are eastward for zonal wind and northward for meridional wind.

eastward in the summer and westward in the winter; their vertical structures, however, are quite different, especially in winter. Unlike the temperature comparison, the "ref" version is qualitatively more similar to what the lidar observed, with the same peak zonal wind during the summer, but its summer-winter contrast below 90 km is less dramatic than what is observed. The difference in zonal wind between the "uns" version of WACCM3 and the lidar data is significant. In this version of WACCM3, although the wind direction is the same, the peak magnitude of the zonal wind is much larger than that of the lidar observations, 71 m/s at 102 km versus 48m/s at 94 km in summer, and −42 m/s at 99 km versus −23 m/s at 102 km in winter. We would expect the zonal wind to change its direction in the mesopause region because of the body force produced by the dissipation of the gravity waves that are propagating upward from the troposphere. However, in this "uns" version of WACCM3, the zonal wind reverses its direction at ∼60 km (not shown) during the winter, which is about 30 km below the reversal observed by lidar. Next, we consider the meridional wind (Figures 3g–3i). The model results exhibit the general trends of the observation, revealing the balance between the Coriolis force and the body force resulting from the deposition of momentum of upward propagating gravity waves, leading to a prevailing meridional flow from the summer pole to the winter pole. The observed southward wind in summer is stronger than the model predicts though. If one examines the model data at lower altitudes, it is clear that the altitudes of meridional wind extremes in both of the model's versions are lower than those observed. For example, the summer maximum meridional wind speed at 86 km in the lidar observation corresponds to minima located at 76 km in the "ref" version, and at 81 km in the "uns" version. Both zonal mean simulations captured the apparent asymmetry between spring and autumn in meridional wind revealed by the lidar observation.

[17] In summary, the comparison of WACCM3 to the lidar data shows that the altitude of the summer mesopause in WACCM is low, and the "uns" simulation shows a mesopause somewhat higher and colder than the "ref." Differences between the two simulations and the observation, in both mesopause altitudes and zonal wind magnitudes, suggest that the properties of the source spectrum (its magnitude and spectral character) are critical in order to simulate a realistic mesopause.

5.2. Comparison of Lidar Observations With HAMMONIA

[18] The HAMMONIA (Figures 4a, 4d, and 4g) temperature monthly mean contour plot (Figures 4a–4c) shows a seasonal variation that is quite similar to the lidar observation. However, the summer mesopause temperature is about 10 K colder in HAMMONIA than in the lidar data and its altitude is about 3 km lower in this model, compared to 3 and 8 km in the "uns" and "ref" versions of WACCM3. The winter mesopause in HAMMONIA is 1 km higher and 11 K warmer than in the lidar data. For the zonal wind field (Figures 4d–4f), the altitude of the observed peak zonal wind in summer and that of the zonal wind reversal in winter are well predicted by HAMMONIA within 1 km or 2.5 km, respectively. During summer, both indicate the

Table 2. Observation and Model Comparisons

	Summer Mesopause			Winter Mesopause			Summer Peak Zonal Wind			Winter Zonal Wind Reversal		Summer Peak Meridional Wind		
Instrument	T, K	z, km	Month	T, K	z, km	Month	u, m s^{-1}	z, km	Month	Altitude, km	Month	u, m s^{-1}	z, km	Month
Lidar[a]	167.4 ± 0.7	84	Jun	173.2 ±1.0	101	Jan	47.6±2.3	94	Jun	95.5±1.0	Dec–Jan	−16.8±1.9, −14.9±2.3	86, 84	May, Jun
WACCM, uns[b]	168.6	81 (80)	Jun	197.4	99 (97.5)	Dec	71.4	102 (100)	Jul	62.5 (62.5)	Dec–Jan	−12.7	81 (80)	Jun
WACCM, ref[b]	169.9	76 (76)	Jun	191.9	99 (97.5)	Jan	48.3	83.5 (82.5)	Jun	88.5 (87.5)	Dec–Jan	−12.6	76 (76)	Jun
HAMMONIA[b]	157.6	81	Jun	184.1	102	Dec	74.8	93	Jul	93	Dec–Jan	−16.6	81	Jun
TIME-GCM[b]	160.7	83 (82)	Jul	182.2	100 (98)	Dec	29.4	95 (94)	Jul	104 (102)	Dec–Jan	−10.7	81 (80)	Jun

[a]Geometric altitude.
[b]Equivalent geometric altitude. Altitudes within the brackets are geopotential height.

reversal altitude at 83 km. However, the value of summer peak zonal wind predicted by HAMMONIA (about 75 m/s), while comparable to the "uns" simulation of WACCM, is considerably larger than that observed by the lidar (48 m/s). In the meridional wind comparison (Figures 4g–4i), the HAMMONIA (Figures 4a, 4d, and 4g) again predicts the same seasonal variation as observed by the lidar with a comparable maximum wind speed, but at a lower altitude relative to the lidar observation.

5.3. Comparison of Lidar Observations With TIME-GCM

[19] Even though the TIME-GCM is quite different from the other two models considered in this work, the TIME-GCM 2003 simulation (Figures 4c, 4f, and 4i) predicts a seasonal variation of temperature similar to that of HAMMONIA, except that the summer mesopause altitude is 1 km lower (but ~7 K colder) than what the lidar observes as compared to 3 km lower and 10 K cooler for HAMMONIA. It is interesting to notice that, compared to both the HAMMONIA and TIME-GCM, the lidar measures a warmer (colder) summer (winter) mesopause temperatures. For zonal wind seasonal variations, TIME-GCM predicts almost the same summer zonal wind peak altitude, but with a peak eastward wind speed (~30 m/s) much slower than both the lidar observation and the HAMMONIA prediction. The TIME-GCM 2003 simulation shows that the zonal wind reverses its direction at about 84 km during the summer and at about 104 km in the winter; they are the same and about 10 km higher, respectively, than lidar observation. The TIME-GCM model shows an abrupt change in zonal wind magnitude during both the spring and autumn equinoxes, whereas the corresponding magnitude changes are not as dramatic as in either the HAMMONIA prediction and lidar observation. Compared to the observed meridional winds, the TIME-GCM result (Figures 4c, 4f, and 4i) shows a seasonal variation with higher spring-autumn symmetry and less variability compared to lidar and other models.

[20] We note that hydrostatic equilibrium is built into the models (that is, the vertical momentum equation is replaced by the hydrostatic equation), but geostrophic balance is not. However, geostrophic balance has been shown to be generally valid for in the midlatitude mesopause region [*Lieberman*, 1999; *Oberheide et al.*, 2002]. Therefore, at midlatitudes winds and temperatures ld approximately be consistent with geostrophic balance. However, since the relationship involves a horizontal derivative of temperature, we are unable to evaluate horizontal gradient of temperature from measurements at a single site, and thus are unable to determine whether the thermal wind relationship is valid from data. The assessment on the implication of geostrophic balance on model-data comparison between wind and temperature is not straightforward.

6. Discussion and Conclusion

[21] On the basis of 120 full-diurnal-cycle observations of the mesopause region, well distributed throughout the year, we present monthly mean temperature, zonal wind and meridional wind with the tidal period perturbations removed. The results are in qualitative agreement with our current understanding of the mesopause region thermal and dynamical structure. The observed monthly mean mesopause region temperature, zonal and meridional winds between 76 and 104 km are tabulated in Tables 1a–1c at 1 km interval. The observations are compared to three general circulation models, WACCM, HAMMONIA and TIME-GCM. In general, the models captured the structure of the two-level mesopause [*She and von Zahn*, 1998] with sharp winter-summer transitions in all three dynamical fields. However, some discrepancies exist between models and observation as well as among model predictions. For example: the summer mesopause altitude observed by the CSU lidar, 84 km, is about 3 and 8 km higher in geometric altitude than the predictions of WACCM3 "uns" and "ref" simulations, respectively; it is 3 km higher than the HAMMONIA and 1 km higher than TIME-GCM predictions. The observed winter mesopause temperature, 173 K, is about 19 (24) K cooler than the prediction of WACCM3 "ref" ("uns"), but only ~10 K cooler than TIME-GCM and HAMONNIA predictions. Owing partially to the difference in model's data set presentation (zonal mean versus a single location), detailed examination of the difference contours between observation and models in temperature and zonal/meridional wind is not warranted at this stage of model development. However, quantitative comparisons that capture the major differences can be made in terms of summer and winter mesopause altitude and temperature, summer peak zonal wind magnitude and altitude, altitude of winter zonal wind reversal, and summer peak meridional wind magnitude and altitude. These differences are summarized

in Table 2 with 1σ-uncertainty of lidar observation given. Not shown in Table 2 is the apparent seasonal asymmetry with higher degree of variability in the observed meridional wind. This observed variability is likely due to planetary waves initiated near the Earth surface that impact the general circulation above. In this regard, a free running GCM, like WACCM3 and HOMMONIA, with the planetary wave effects generated self-consistently from lower-atmosphere dynamics, may yield a higher degree of variability and seasonal asymmetry, thereby closer to the observed variability than a model, like TIME-GCM, with planetary wave influences forced at the lower boundary by daily input of NCEP reanalysis.

[22] Because mesospheric dynamics are believed to be controlled largely by gravity wave behavior, the differences in gravity wave input between these three models are significant. Not only are the schemes for gravity wave parameterization different (WACCM and TIME-GCM use Lindzen's scheme, while HAMONNIA uses Hines' scheme), their launch altitudes are also different (at 700 hPa, 500 hPa and 10 hPa for HAMONNIA, WACCM and TIME-GCM, respectively). The tuning of gravity wave spectra giving rise to different wind filtering, could lead to a difference between the different simulations in WACCM as large as that between different models. The difference in PW influences among models can change the longitudinal distribution of GW forcing because of the fact that PWs modify the stratospheric winds and thus alteri the filtering of GWs, as they propagate upward [*Dunkerton and Butchart*, 1984; *Smith*, 1996]. Therefore PW filtering also provides a possibility for the differences among models, more so in winter, since the quasi-stationary PW cannot propagate through summer easterlies. All of these complications could result in differences between models, and model-observation in a way difficult to sort out without further and more focused model studies.

[23] The full-diurnal-cycle observations by the Na lidar at Colorado State University contain enough data in a 4-year period to provide tidal-removed mesopause region monthly mean temperature and horizontal wind, and to derive the seasonal variations in the mean state of these fields. It is evident that the uncertainty bars for lidar-observed mean temperature, zonal and meridional winds are smaller than both model-lidar and intermodel discrepancy, suggesting that at this stage of model development, the gravity wave parameterizations and other interactive inputs to the model still need to be improved and fine-tuned to produce more realistic predictions. However, all three models do capture the general altitude and seasonal structure of the mesopause region, as observed by lidar. Some models, like HAMMONIA and TIME-GCM, appear to outperform WACCM3 in this comparison. On the other hand, the source spectrum approach, along with the ability to shift the maximum stress to specific gravity wave phase speed, shows that improvements to the WACCM3 model are possible as well.

[24] Comparative studies between observations and models, which provide a reality check, are useful and necessary steps in model evaluation and improvement, as already demonstrated by plots comparing winds between TIME-GCM and ground-based (radar) and satellite (UARS/HRDI) observations [*Roble*, 2000]. Although we are comparing observations from one on within a certain region of Earth atmosphere with global-scale whole atmospheric models, this type of comprehensive study is very useful in terms of model evaluation, and more comparisons are needed. This comparative study with both temperature and horizontal wind fields is the first step to reveal the importance of full-diurnal-cycle observation on the one hand, and the differences between models and observations as well as those between different models, on the other. The conclusion that the models capture the main features of the observations supports our understanding of the basic atmospheric processes, whereas the discrepancies reveal the physical differences between different models and at the same time provide guidance to fine-tune and improve the parameterization of gravity wave sources and spectra of each model presented here.

[25] **Acknowledgments.** The work is supported in part by grants from NASA, NAG5-13567 and NNX07AB64G, and from National Science Foundation, ATM-0545221 and ATM-0335127. The National Center for Atmospheric Research is supported by the National Science Foundation. T.Y., C.Y.S. and D.A.K. thank Steve Reising for critical reading and editing of the manuscript. R. G. Roble and H.-L. Liu's efforts are in part supported by the Office of Naval Research (N00014-07-C0209).

References

Arnold, K. S., and C. Y. She (2003), Metal fluorescence lidar (light detection and ranging) and the middle atmosphere, *Contemporary Phys.*, *44*, 35–49.

Chen, S. S., Z. L. Hu, M. A. White, D. A. Krueger, and C. Y. She (2000), Lidar observations of seasonal variation of diurnal mean temperature in the mesopause region over Fort Collins, CO (41°N, 105°W), *J. Geophys. Res.*, *105*, 12,371–12,380.

Crary, D. J., and J. M. Forbes (1983), On the extraction of tidal information from measurements covering a fraction of a day, *Geophys. Res. Lett.*, *10*, 580–582.

Dunkerton, T. J., and N. Butchart (1984), Propagation and selective transmission of internal gravity waves in a sudden warming, *J. Atmos. Sci.*, *41*, 1443–1660.

Fomichev, V. I., and G. M. Shved (1998), Net radiative heating in the middle atmosphere, *J. Atmos. Terr. Phys.*, *50*, 671–688.

Franke, S. J., and D. Thorsen (1993), Mean winds and tides in the upper middle atmosphere at Urbana (40°N, 88°W) during 1991–92, *J. Geophys. Res.*, *98*, 18,607–18,615.

Garcia, R. R., R. Lieberman, J. M. Russell III, and M. G. Mlynczak (2005), Large-scale waves in the mesosphere and lower thermosphere observed by SABER, *J. Atmos. Sci.*, *62*, 4384–4399.

Garcia, R. R., D. R. Marsh, D. E. Kinnison, B. A. Boville, and F. Sassi (2007), Simulation of secular trends in the middle atmosphere, 1950–2003, *J. Geophys. Res.*, *112*, D09301, doi:10.1029/2006JD007485.

Hagan, M. E., R. G. Burage, J. M. Forbes, H. Hackney, W. J. Randel, and X. Zhang (1999), GSWM-98: Results for migrating solar tides, *J. Geophys. Res.*, *104*, 6813–6828.

Hines, C. O. (1997a), Doppler-spread parameterization of gravity wave momentum deposition in the middle atmosphere. Part 1: Basic formulation, *J. Atmos. Sol. Terr. Phys.*, *59*, 371–386.

Hines, C. O. (1997b), Doppler-spread parameterization of gravity wave momentum deposition in the middle atmosphere. Part 2: Broad and quasi monochromatic spectra, and implementation, *J. Atmos. Sol. Terr. Phys.*, *59*, 387–400.

Jacobi, C., Y. I. Portnyagin, E. G. Merzlyakov, T. V. Solovjova, N. A. Makarov, and D. Kürschner (2005), A long-term comparison of mesopause region wind measurements over Eastern and Central Europe, *J. Atmos. Sol. Terr. Phys.*, *67*, 229–240.

Jarvis, M. J. (2001), Bridging the atmosphere divide, *Science*, *293*(5538), 2218–2219, doi:10.1126/science.1064467.

Kinnison, D. E., et al. (2007), Sensitivity of chemical tracers to meteorological parameters in the MOZART-3 chemical transport model, *J. Geophys. Res.*, *112*, D20302, doi:10.1029/2006JD007879.

Lawrence, A. R., and M. J. Jarvis (2001), Initial comparisons of planetary waves in the stratosphere, mesosphere and ionosphere over Antarctica, *Geophys. Res. Lett.*, *28*, 203–206.

Leblanc, T., I. S. McDermid, P. Keckhut, A. Hauchecorne, C. Y. She, and D. A. Krueger (1998), Temperature climatology of the middle atmosphere from long-term lidar measurements at mid- and low-latitudes, *J. Geophys. Res.*, *103*, 17,191–17,204.

Lieberman, R. S. (1999), The gradient wind in the mesosphere and lower thermosphere, *Earth Planets Space*, *51*, 751–761.

Lindzen, R. S. (1981), Turbulence and stress owing to gravity wave and tidal breakdown, *J. Geophys. Res.*, *86*, 9707–9714.

Liu, H.-L., and R. G. Roble (2002), A study of a self-generated stratospheric sudden warming and its mesospheric-lower thermospheric impacts using the coupled TIME-GCM/CCM3, *J. Geophys. Res.*, *107*(D23), 4695, doi:10.1029/2001JD001533.

Liu, H.-L., and R. G. Roble (2005), Dynamical coupling of the stratosphere and mesosphere in the 200 2 Southern Hemisphere major stratospheric sudden warming, *Geophys. Res. Lett.*, *32*, L13804, doi:10.1029/2005GL022939.

Lübken, F.-J. (1999), Thermal structure of the arctic summer mesopause, *Geophys. Res. Lett.*, *104*, 9135–9149.

Lübken, F.-J., and U. von Zahn (1991), Thermal structure of the mesopause region at polar latitudes, *J. Geophys. Res.*, *96*, 20,841–20,857.

Manson, A. H., et al. (1989), Climatologies of semi-diurnal and diurnal tides in the middle atmosphere (70–110 km) at middle latitudes (40–50), *J. Atmos. Terr. Phys.*, *51*, 579–593.

McLandress, C., G. G. Shepherd, and B. H. Solheim (1996), Satellite observations of thermospheric tides: Results from the Wind Imaging Interferometer on UARS, *J. Geophys. Res.*, *101*, 4903–4114.

Mlynczak, M. G., and S. Solomon (1993), A detailed evaluation of heating efficiency in the middle atmosphere, *J. Geophys. Res.*, *98*, 10,517–10,541.

Oberheide, J., G. A. Lehmacher, D. Offermann, K. U. Grossmann, A. H. Manson, C. E. Meek, F. J. Schmidlin, W. Singer, P. Hoffmann, and R. A. Vincent (2002), Geostrophic wind fields in the stratosphere and mesosphere from satellite data, *J. Geophys. Res.*, *107*(D23), 8175, doi:10.1029/2001JD000655.

Pancheva, D., et al. (2002), Global-scale tidal structure in the mesosphere and lower thremosphere during PSMOS campaigns of June–August 1999 and comparison with the globa-scale wave model, *J. Atmos. Sol. Terr. Phys.*, *64*, 1011–1035.

Roble, R. G. (2000), On the feasibility of developing a global atmospheric model extending from the ground to the exosphere, in *Atmospheric Science Across the Stratoapuse*, *Geophys. Monogr. Ser.*, vol. 123, edited by D. E. Siskind, S. D. Eckermann, and M. E. Summers, pp. 53–67, AGU, Washington, D. C.

Roeckner, E., R. Brokopf, M. Esch, M. Giorgetta, S. Hagemann, L. Kornblueh, E. Manzini, U. Schlese, and U. Schulzweida (2006), Sensitivity of simulated climate to horizontal and vertical resolution in the ECHAM5 atmosphere model, *J. Clim.*, *19*, 3771–3791.

Schmidt, H., G. P. Brasseur, M. Charron, E. Manzini, M. A. Giorgetta, T. Diehl, V. I. Fomichev, D. Kinnison, D. Marsh, and S. Walters (2006), The HAMMONIA chemistry climate model: Sensitivity of the mesopause region to the 11-year solar cycle and CO_2 doubling, *J. Clim.*, *19*, 3903–3931.

She, C. Y., and U. von Zahn (1998), The concept of two-level mesopause: Support through new lidar observation, *J. Geophys. Res.*, *103*, 5855–5863.

She, C. Y., S. S. Chen, Z. L. Hu, J. Sherman, J. D. Vance, V. Vasoli, M. A. White, J. R. Yu, and D. A. Krueger (2000), Eight-year climatology of nocturnal temperature and sodium density in the mesopause region (80 to 105 km) over Fort Collins, CO (41°N, 105°W), *Geophys. Res. Lett.*, *27*, 3289–3292.

She, C. Y., et al. (2003), The first 80-hour continuous lidar campaign for simultaneous observation of mesopause region temperature and wind, *Geophys. Res. Lett.*, *30*(6), 1319, doi:10.1029/2002GL016412.

She, C. Y., et al. (2004), Tidal perturbations and variability in the mesopause region over Fort Collins, CO (41N, 105W): Continuous multi-day temperature and wind lidar observations, *Geophys. Res. Lett.*, *31*, L24111, doi:10.1029/2004GL021165.

Smith, A. K. (1996), Longitudinal variations in mesospheric winds: Evidence for gravity wave filtering by planetary waves, *J. Atmos. Sci.*, *53*, 1156–1173.

States, R. J., and C. S. Gardner (1998), Influence of the diurnal tide and thermosphere heat sources on the formation of mesospheric temperature inversion layers, *Geophys. Res. Lett.*, *25*, 1483–1486.

States, R. J., and C. S. Gardner (2000), Temperature structure of the mesopause region (80–105 km) at 40(N latitude: 1. Seasonal variation, *J. Atmos. Sci.*, *57*, 66–77.

Swinbank, R., and D. A. Ortland (2003), Compilation of wind data for the Upper Atmosphere Research Satellite (UARS) Reference Atmosphere Project, *J. Geophys. Res.*, *108*(D19), 4615, doi:10.1029/2002JD003135.

von Zahn, U., and J. Höffner (1996), Mesopause temperature profiling by potassium lidar, *Geophys. Res. Lett.*, *23*, 141–144.

Yu, J. R., and C. Y. She (1995), Climatology of a mid-latitude mesopause region observed by Na lidar at Ft. Collins, CO (40.6°N, 105°W), *J. Geophys. Res.*, *100*, 7441–7452.

Yuan, T., et al. (2006), Seasonal variation of diurnal perturbations in mesopause region temperature, zonal, and meridional winds above Fort Collins, Colorado (40.6°N, 105°W), *J. Geophys. Res.*, *111*, D06103, doi:10.1029/2004JD005486.

R. Garcia, H.-L. Liu, R. G. Roble, and F. Sassi, National Center for Atmospheric Research, Boulder, CO 80307, USA.

D. A. Krueger, C.-Y. She, and T. Yuan, Physics Department, Colorado State University, Fort Collins, CO 80523-1875, USA. (titus@lamar.colostate.edu)

H. Schmidt, Max Planck Institute for Meteorology, D-20146 Hamburg, Germany.